第38卷第1期
2019年2月

红外与毫米波学报
J. Infrared Millim. Waves

Vol. 38, No. 1
February, 2019

文章编号: 1001-9014(2019)01-0003-05

DOI: 10.11972/j.issn.1001-9014.2019.01.001

Atomic-Layer-Deposited ultrathin films of vanadium pentoxide crystalline nanoflakes with controllable thickness and optical band-gap

ZHANG Tian-Ning[1,2], WANG Shu-Xia[1], HUANG Tian-Tian[1], WEI Wei[1], CHEN Xin[1,2*], DAI Ning[1,2]

(1. State Key Laboratory for Infrared Physics, Shanghai Institute of Technical Physics, Chinese Academy of Sciences, Shanghai 200083, China;
2. University of Chinese Academy of Sciences, Beijing 100049, China)

Abstract: Thin films of crystalline V_2O_5 nanoflakes were prepared through atomic layer deposition (ALD) process. The film thickness was verified to play a critical role in determining structural morphology, optical bandgap and Raman vibration of crystalline V_2O_5 thin films. Two optical bandgaps observed at about 2.8 eV and 2.4 eV result from two growth stages during ALD preparation. We expect that these results help to understand the growth control of ultrathin films and their functional devices.

Key words: atomic layer deposition, vanadium pentoxide, thin films
PACS: 78.20.-e

厚度与带隙可调、原子层沉积的超薄五氧化二钒纳米晶薄膜

张天宁[1,2], 王书霞[1], 黄田田[1], 魏 威[1], 陈 鑫[1,2*], 戴 宁[1,2]
(1. 中国科学院上海技术物理研究所 红外物理国家重点实验室, 上海 200083;
2 中国科学院大学, 北京 100049)

摘要: 利用原子层沉积方法制备 V_2O_5 纳米片晶薄膜. 薄膜厚度可以被精确控制, 并对纳米晶 V_2O_5 薄膜的结构形貌、光学带隙和拉曼振动有显著影响. 原子层沉积过程中 V_2O_5 薄膜生长的两个阶段导致薄膜具有两个光学带隙, 这将有助于理解超薄薄膜生长与功能应用.

关 键 词: 原子层沉积; 五氧化二钒; 薄膜
中图分类号: O484.1 **文献标识码:** *A*

Introduction

Two-dimensional layered transition metal oxides have attracted considerable attention due to their intriguing chemical activity, distinctive electrical and optical properties. The layered nanostructures have shown promises in facilitating functional devices including optical [1] and electronic devices [2], sensors [3], and rechargeable lithium batteries [4,5]. Among these layered transition metal oxides, layered V_2O_5 materials have been widely investigated due to its low cost, nature abundance and high charge storage capability. Some investigations have recently demonstrated V_2O_5-based electrochromism [6-9], photocatalysis [10-12], sensor [13], and energy storage [14-18]. Crystalline V_2O_5 thin films play a vital role in improving the performances of functional electrodes [19, 20]. In order to optimize electronic or ionic conductivity, the nanoscale thicknesses of V_2O_5 films are controlled to improve ionic diffusion [21] and electronic transportation [22, 23]. In general, the film thicknesses of layered V_2O_5 materials intensely affect their optical and electrical properties. It is known that atomic layer deposition (ALD) is an excellent technique to precisely control the thickness of functional films on complicated configurations [24]. In this paper, we present the preparation of crystalline V_2O_5 thin films with controllable thickness of several nanometers through an ALD process at low temperature. The investigations focus on the relationships between the film thickness and surface morphology, optical bandgap and pho-

Received date: 2018-02-10, **revised date:** 2018-12-25 **收稿日期:** 2018-02-10, **修回日期:** 2018-12-25
Foundation items: Supported by the National Key R&D Program of China (2016YFA0202200) and Youth Innovation Promotion Association, CAS
Biography: ZHANG Tian-Ning (1989-), male, Liaoning, Ph. D. Research interests are atomic layer deposition. E-mail: tnzhang@mail.sitp.ac.cn
* **Corresponding author:** E-mail: xinchen@mail.sitp.ac.cn

non vibration of crystalline V_2O_5 thin films. Meanwhile, the distinctions between the initial stage and the follow-up stage are discussed to reveal the growth process of V_2O_5 ultrathin films during the ALD process.

1 Experiments

V_2O_5 thin films were deposited on the silicon or silica substrates by using oxygen plasma and triisopropoxy-vanadium oxide (VTOP) as precursors in an ALD reactor (Picosun-R200) at 200°C. N_2 and Ar were used as carrier gases for oxygen plasma and VTOP respectively. When the pressure was 80 Pa in the ALD chamber, the pulse time of VTOP and oxygen plasma were 0.7 s and 1.5 s respectively.

The surface morphologies were examined by atomic force microscopy (AFM, NT-AIST) in a tapping mode. Scanning electron microscopy (SEM) images were obtained on FEI Sirion200, and transmission electron microscopy (TEM) images were obtained on JOEL JEM-2100F performed at an accelerated voltage of 200 kV. X-ray photoelectron spectroscopy (XPS; Axis Ultra DLD) was used for elements analysis. X-ray diffraction (XRD) patterns were collected on Bruker D8 with a monochromatic source of Cu-Ka radiation ($\lambda = 0.154\ 18$ nm) at 1.6 kW (40 kV, 40 mA). Raman spectra were obtained using TII Tokyo-Nanofinder 30 at room temperature. Spectroscopic ellipsometry (SE) was performed on J. A. Woollam-M2000X-FB-300XTF at an incident angle of 65°. UV-Vis-NIR absorption spectra were measured using PerkinElmer-Lamda 950 spectroscopy with an integration sphere accessory.

2 Results and discussions

Fig. 1 shows SEM and AFM images of V_2O_5 thin films deposited with different thicknesses by controlling ALD cycle numbers on silicon substrates. The representative surface morphology is related to the film thicknesses with different ALD cycle numbers. When the thickness is less than 1 500 ALD cycles, the films are with smooth surface, as shown in Fig. 1a and 1b. As the films thickness increases, the small grains grow up and finally evolve into orthorhombic shaped crystallites (Fig. 1c-e). The crystal nucleation and growth may determine the surface morphologies of V_2O_5 thin films due to the formation of V_2O_5 nanoflakes during ALD procedure [25, 26]. The use of O_2 plasma leads to the crystalline nanoplates with sharp-shaped edges.

Stoichiometric ratio is critical for vanadium oxides to determine the crystalline structure and morphology. Thus, XPS and XRD were utilized to investigate the compositions and structures of thin films with different thicknesses (Fig. 2). The Binding energies at about 517.24 and 524.68 eV result from $2p_{3/2}$ and $2p_{1/2}$ of vanadium element. There is an energy difference of nearly 7.4 eV between V $2p_{3/2}$ and $2p_{1/2}$, which implies the existence of V^{+5} oxidation state [27]. In addition, the V^{+4} oxidation state is not detected in XPS. All these results suggest the formation of V_2O_5 thin films during ALD procedure. For two thin films with thicknesses of 500 and 2000 ALD cycles, the band energies of V 2p are almost the same. However, except for O 1s peak at 530.36 eV, there is an obvious peak at a binding energy of ~532.1 eV (Figure 2b) in the case of the films with a thickness of 500 ALD cycles. This result may be related to H_2O molecules absorbed in the films, and the thinner films are easily affected by the adsorbed molecules.

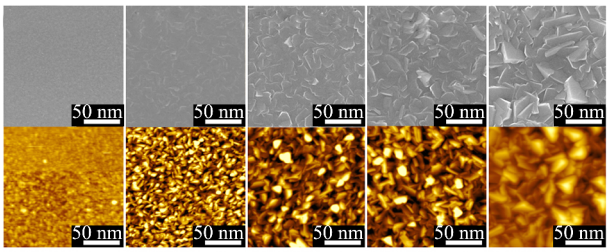

(a)300cycles (b)1500cycles (c)3000cycles (d)4500cycles (e)7500cycles

Fig. 1 Top-view SEM (up) and AFM (down) images of V_2O_5 thin films with varying thicknesses of (a) 300, (b) 1 500, (c) 3 000, (d) 4 500, (e) 7 500 ALD cycles

图1 不同厚度五氧化二钒的SEM(上部)和AFM(下部)表面形貌:(a) 300循环(b) 1 500循环(c) 3 000循环(d) 4 500循环(e) 7 500循环

Fig. 3 shows Raman spectra of the lattice variations in V_2O_5 thin films with different thicknesses. For all the V_2O_5 films with different thicknesses by varying ALD cycles, Raman shifts at 102, 145, 197, 284, 405, 484, and 700 cm^{-1} are in agreement with those previously reported [28]. The intensity of Raman peak rises as the thickness of V_2O_5 film increases (Fig. 3a). The Raman shifts at 303 and 526 cm^{-1} are indistinguishable because the Si substrates have obvious Raman shifts at about 300 and 520 cm^{-1}. Raman shifts at 145 cm^{-1} are the most obvious and come from a mixture of B_{1g} and B_{3g} vibrations. The B_{1g} and B_{3g} modes correspond to the shear and rotation motion of V-O_B bond ladders, respectively (Fig. 3e) [28]. This bending mode is strongly associated with the layered structure [29]. There is a slight blue-shift at 145 cm^{-1} when the thickness of V_2O_5 thin film decreases from 1 500 cycles to 300 cycles, which indicates the presence of a little strain occurred in the initial growth stage of the layered thin films (Fig. 3b). This observed shift may result from small compression strain along c-axis in the layered V_2O_5 structure reported elsewhere [30, 31]. No detectable changes are found in Fig. 3c and 3d.

As mentioned above, for thin films with varied thicknesses, the surface morphology and XPS spectra are different. Thus, spectroscopic ellipsometry (SE), cross-sectional SEM and TEM measurements are further performed to understand the essential growth process of V_2O_5 ultrathin films. Fig. 4a shows the relationship between the thickness and ALD cycle number. The thicknesses are obtained from SE and SEM measurements. As shown in Fig. 2f, there is a silica layer with about 2 nm between silicon substrate and V_2O_5 thin film. Thus, a three-layer model is used in SE data and analysis. Moreover, the surface roughness is also considered in SE a-

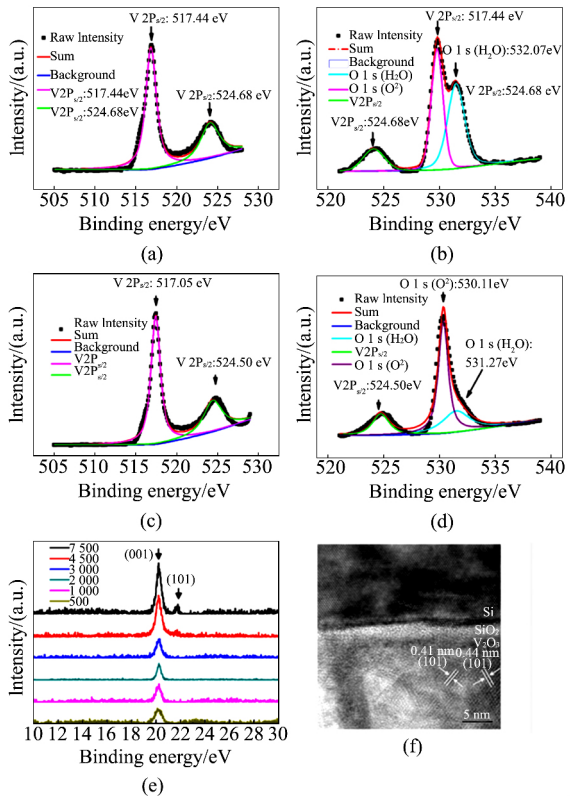

Fig. 2　(a, b) V $2p_{3/2}$ and O 1s peaks of XPS spectra for V_2O_5 films with a thickness of 500 ALD cycles, respectively, and (c, d) with a thickness of 2 000 ALD cycles. (e) XRD patterns of V_2O_5 films with varying thickness; (f) TEM image of V_2O_5 films with a thickness of 2000 ALD cycles

图 2　(a, b) 500 循环五氧化二钒薄膜的 V $2p_{3/2}$ 和 O 1s 的 XPS 谱,(c, d) 2 000 循环五氧化二钒薄膜的 V $2p_{3/2}$ 和 O 1s 的 XPS 谱,(e) 不同厚度五氧化二钒的 XRD 谱图(f) 2 000ALD 循环五氧化二钒薄膜的 TEM 图

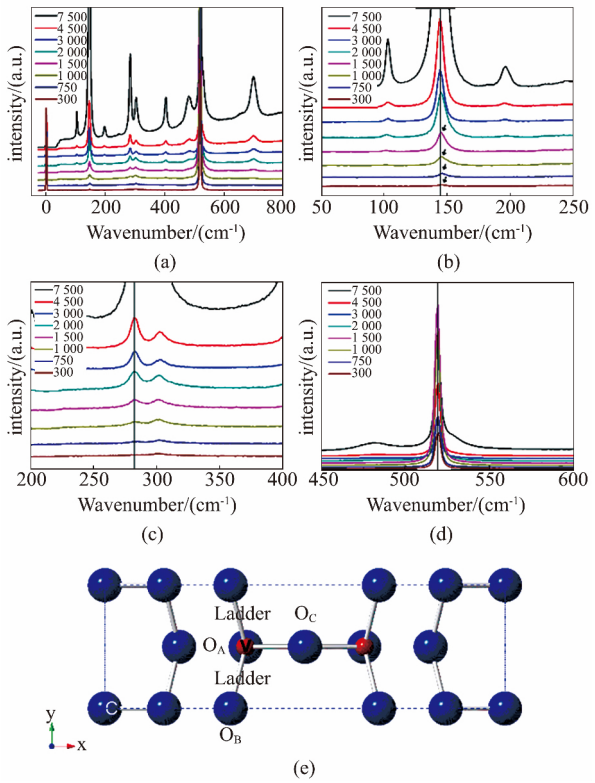

Fig. 3　(a) Raman spectra of V_2O_5 films with various thicknesses; (b, c, d) a zoom at the ranges of 50 ~ 250 cm^{-1}, 200 ~ 400 cm^{-1} and 450 ~ 600 cm^{-1}, respectively. (e) Schematic molecular structure of V_2O_5

图 3　(a) 不同厚度五氧化二钒薄膜的拉曼图谱,(b, c, d) 50 ~ 250 cm^{-1}, 200 ~ 400 cm^{-1} 和 450 ~ 600 cm^{-1} 的局部放大,(e) 五氧化二钒的分子结构模型

nalysis and can be obtained from the RMS roughness in AFM measurements. For example, for the V_2O_5 film prepared with 7 500 ALD cycles, we can use SE simulation to obtain a thickness of 215 nm, which is also verified by cross-sectional SEM measurements. Fig. 4a suggests the effective thickness increases linearly with ALD cycles. In the range from 1 500 to 7 500 cycles, the growth rate is about 0.3 Å/cycle. However, the growth rate is about 0.2 Å/cycle in the range from 100 to 1 500 cycles. The ratio of Rms roughness to thickness remains relatively stable although the Rms roughness increases with the increasing ALD cycles, as shown in Fig. 4b. The variation trends of both growth rate and surface morphology indicate that there are two growth stages during the formation of V_2O_5 thin films, which may be understood with the Stranski-Krastanov growth mode [32]. Once the film thickness is up to a critical thickness, the growth modes change from the layer growth to the island-based growth. In the initial layer growth stage, the V_2O_5 films are very thin and almost parallel to surface by the reaction between ALD precursors and substrates. The growth is self-limiting on the substrate, which results in a low surface roughness. Once the V_2O_5 ultrathin films form, the precursor molecules are easily adsorbed and selectively reacted with V_2O_5 nanoflakes, which leads to an improved growth rate and an island-based growth mode.

Fig. 5 displays Tauc plots derived from SE and UV-Vis-NIR absorption spectra. The V_2O_5 ultrathin film has an indirect bandgap, and the bandgap red-shifts from 2.66 eV to about 2.40 eV when the thickness increases from 50 to 300 cycles (Fig. 5a). Furthermore, Figure 3c suggests a bandgap of 2.36 eV for the thin film with a thickness of 500 ALD cycles prepared on quartz substrate, which is in agreement with SE simulation. The red-shift can be attributed to the quantum size effect. Once the thicknesses increase up to more than 1000 ALD cycles, two bandgaps are identified as shown in Fig. 3b and 3d. One stays at 2.40 eV and the other varies from 2.73 eV to 2.90 eV. The formation of two bandgaps might result from the two growth stages mentioned above. In the layer growth stage the bandgap decreases with the thickness increasing. Then, the thin film subsequently grows up and another bandgap appears while the primary bandgap of the initial ultrathin film remains. Small grains form in the thin films during the island-based growth stage, which leads to a larger bandgap. All these results

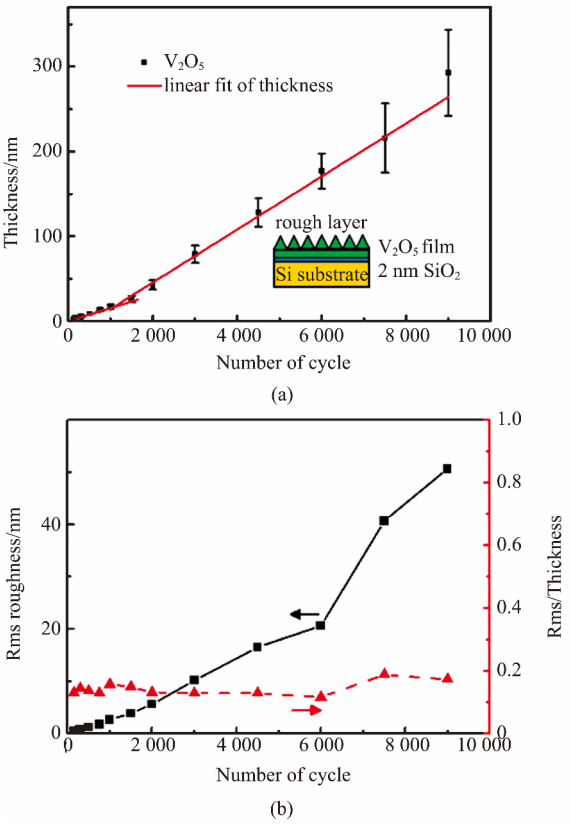

Fig. 4 (a) Relationship between thickness and ALD cycle numbers, the inset shows the schemtic structure of thin film deposited on the Si substrate. (b) Plots for the relationships between Roughness and roughness-thickness ratio and ALD cycle numbers

图4 (a) 厚度和 ALD 循环数的关系,插入图为硅衬底上五氧化二钒薄膜的模型结构示意图,(b) 表面粗糙度及粗糙度膜厚比值与 ALD 循环数的关系图

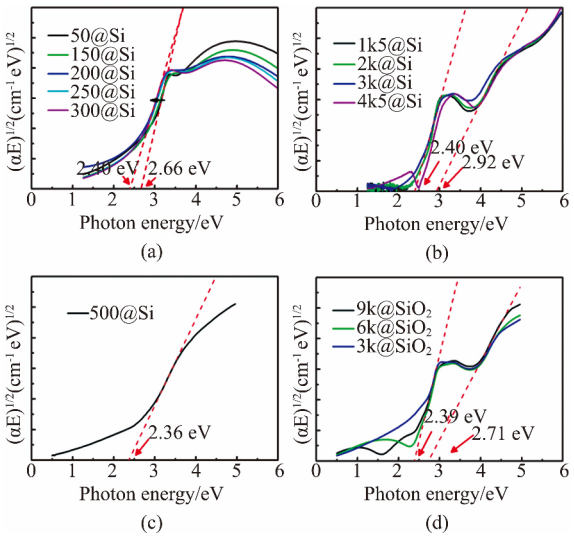

Fig. 5 Tauc plots of V_2O_5 films with various thicknesses of (a) 50 to 300 ALD cycles on Si substrates; (b) 1 500 to 4 500 ALD cycles on Si substrates; (c) 500 ALD cycles on quartz substrates; (d) 3 000, 6 000 and 9 000 ALD cycles on quartz substrates

图5 不同厚度五氧化二钒薄膜的能带吸收关系图:(a) 硅衬底上 50 到 300 ALD 循环的薄膜,(b) 硅衬底上 1 500 到 4 500 ALD 循环的薄膜,(c) 石英衬底上 500 循环 ALD 的薄膜,(d) 石英衬底上 3 000 到 9 000 ALD 循环的薄膜

suggest that the optical properties of V_2O_5 thin film could be adjusted by the control of film thickness during an ALD process.

3 Conclusions

We have successfully prepared V_2O_5 thin films with a thickness down to 5 nm by using ALD process. All investigations on surface morphology, optical bandgap and Raman vibration confirm that the film thickness of crystalline V_2O_5 nanoflakes can be precisely controlled. Meanwhile, the two observed optical bandgaps result from two growth stages during the ALD preparation of crystalline V_2O_5 thin films. We expect that these results will enable us to understand the growth control of ultrathin films and their applications in functional optical and electrochromic devices.

References

[1] Haque F, Daeneke T, Kalantar-zadeh K, *et al*. Two-dimensional transition metal oxide and chalcogenide-Based photocatalysts [J]. *Nano-Micro Letters*, 2018, **10**(2): 23-27.

[2] Granqvist C G, Arvizu M A, Bayrak Pehlivan İ, *et al*. Electrochromic materials and devices for energy efficiency and human comfort in buildings: A critical review [J]. *Electrochimica Acta*, 2018, **259**: 1170-1182.

[3] Varghese S S, Varghese S H, Swaminathan S, *et al*. Two-dimensional materials for sensing: graphene and beyond [J]. *Electronics*, 2015, **4**(3): 651-687.

[4] Cong L N, Xie H M, Li J H. Hierarchical structures based on two-dimensional nanomaterials for rechargeable lithium btteries [J]. *Advanced Energy Materials*, 2017, **7**(12): 1601906.

[5] Mei J, Liao T, Kou L Z, *et al*. Two-dimensional metal oxide nanomaterials for next-generation rechargeable batteries [J]. *Advanced Materials*, 2017, **29**(48): 1700176.

[6] Vernardou D. Using an atmospheric pressure chemical vapor deposition process for the development of V_2O_5 as an electrochromic material [J]. *Coatings*, 2017, **7**(2): 24.

[7] He W, Liu Y, Wan Z, *et al*. Electrodeposition of V_2O_5 on TiO_2 nanorod arrays and their electrochromic properties [J]. *RSC Advances*, 2016, **6**(73): 68997-69006.

[8] Panagopoulou M, Vernardou D, Koudoumas E, *et al*. Tunable Properties of Mg-doped V_2O_5 Thin Films for Energy Applications: Li-ion Batteries and Electrochromics [J]. *Journal of Physical Chemistry C*, 2017, **121**(1): 70-79.

[9] Park H, Kim D S, Hong S Y, *et al*. A skin-integrated transparent and stretchable strain sensor with interactive color-changing electrochromic displays [J]. *Nanoscale*, 2017, **9**(22): 7631.

[10] Shanmugam M, Alsalme A, Alghamdi A, *et al*. Enhanced photocatalytic performance of the graphene-V_2O_5 nanocomposite in the degradation of methylene blue dye under direct sunlight [J]. *ACS Applied Materials & Interfaces*, 2015, **7**(27): 14905-14911.

[11] Epifani M, Kaciulis S, Mezzi A, *et al*. Inorganic photocatalytic enhancement: activated RhB photodegradation by surface modification of SnO_2 nanocrystals with V_2O_5-like species [J]. *Scientific Reports*, 2017, **7**: 46855.

[12] Liu M S, Su B, Tang Y, *et al*. Recent advances in nanostructured vanadium oxides and composites for energy conversion [J]. *Advanced Energy Materials*, 2017, **7**(23): 1700885.
[13] Kumar S, Qadir A, Maury F, *et al*. Visible thermochromism in vanadium pentoxide coatings [J]. *ACS Applied Materials & Interfaces*, 2017, **9**(25): 21447-21456.
[14] Hu P, Yan M Y, Zhu T, *et al*. Zn/V_2O_5 aqueous hybrid-ion battery with high voltage platform and long cycle life [J]. *ACS Applied Materials & Interfaces*, 2017, **9**(49): 42717-42722.
[15] Ma Y N, Huang A B, Zhou H J, *et al*. Template-free formation of various V_2O_5 hierarchical structures as cathode materials for lithium-ion batteries [J]. *Journal of Materials Chemistry A*, 2017, **5**(14): 6522-6531.
[16] Xiao F, Song X X, Li Z H, *et al*. Embedding of Mg-doped V_2O_5 nanoparticles in a carbon matrix to improve their electrochemical properties for high-energy rechargeable lithium batteries [J]. *Journal of Materials Chemistry A*, 2017, **5**(33): 17432-17441.
[17] Yue Y, Liang H. Micro- and nano-structured vanadium pentoxide (V_2O_5) for electrodes of lithium-ion batteries [J]. *Advanced Energy Materials*, 2017, **7**(17): 1602545.
[18] Zhang Y F, Wang H W, Yang J, *et al*. Hydrogenated vanadium oxides as an advanced anode material in lithium ion batteries [J]. *Nano Research*, 2017, **10**(12): 4266-4273.
[19] Mortimer R J. Electrochromic materials [J]. *Chemical Society Reviews*, 1997, **26**(3): 147-156.
[20] Whittingham M S. Lithium batteries and cathode materials [J]. *Chemical Reviews*, 2004, **104**(10): 4271-4301.
[21] Rui X H, Lu Z Y, Yu H, *et al*. Ultrathin V_2O_5 nanosheet cathodes: realizing ultrafast reversible lithium storage [J]. *Nanoscale*, 2013, **5**(2): 556-560.
[22] Brown E, Acharya J, Pandey G P, *et al*. Highly stable three lithium insertion in thin V_2O_5 shells on vertically aligned carbon nanofiber arrays for ultrahigh-capacity lithium ion battery cathodes [J]. *Advanced Materials Interfaces*, 2016, **3**(23): 1600824.
[23] Song Y, Liu T Y, Yao B, *et al*. Amorphous mixed-valence vanadium oxide/exfoliated carbon cloth structure shows a record high cycling stability [J]. *Small*, 2017, **13**(16): 1700067.
[24] Detavernier C, Dendooven J, Sree S P, *et al*. Tailoring nanoporous materials by atomic layer deposition [J]. *Chemical Society Reviews*, 2011, **40**(11): 5242-5253.
[25] Ostreng E, Nilsen O, Fjellvag H. Optical properties of vanadium pentoxide deposited by ALD [J]. *Journal of Physical Chemistry C*, 2012, **116**(36): 19444-19450.
[26] Chen X Y, Pomerantseva E, Gregorczyk K, *et al*. Cathodic ALD V_2O_5 thin films for high-rate electrochemical energy storage [J]. *RSC Advances*, 2013, **3**(13): 4294-4302.
[27] Colton R J, Guzman A M, Rabalais J W. Electrochromism in some thin-film transition - metal oxides characterized by x - ray electron spectroscopy [J]. *Journal of Applied Physics*, 1978, **49**(1): 409-416.
[28] Baddour-Hadjean R, Pereira-Ramos J P, Navone C, *et al*. Raman microspectrometry study of electrochemical lithium intercalation into sputtered crystalline V_2O_5 thin films [J]. *Chemistry of Materials*, 2008, **20**(5): 1916-1923.
[29] Wachs I E, Jehng J M, Hardcastle F D. The interaction of V_2O_5 and Nb_2O_5 with oxide [J]. *Solid State Ionics*, 1989, **32-3**: 904-910.
[30] Ramana C V, Smith R J, Hussain O M, *et al*. Surface analysis of pulsed laser-deposited V_2O_5 thin films and their lithium intercalated products studied by Raman spectroscopy [J]. *Surface and Interface Analysis*, 2005, **37**(4): 406-411.
[31] Sreedhara M B, Ghatak J, Bharath B, *et al*. Atomic layer deposition of ultrathin crystalline epitaxial films of V_2O_5 [J]. *ACS Applied Materials & Interfaces*, 2017, **9**(3): 3178-3185.
[32] Stranski I N, Krastanow L. Zur theorie der orientierten ausscheidung von Ionenkristallen aufeinander [J]. *Monatshefte Für Chemie Und Verwandte Teile Anderer Wissenschaften*, 1937, **71**(1): 351-364.